Surface & Coatings Technology 203 (2009) 3398–3404

Contents lists available at ScienceDirect

Surface & Coatings Technology

journal homepage: www.elsevier.com/locate/surfcoat

Supertough UV-curable silane/silica gas barrier coatings on polymers

Y. Leterrier [a,*], B. Singh [a], J. Bouchet [a], J.-A.E. Månson [a], G. Rochat [b], P. Fayet [b]

[a] Laboratoire de Technologie des Composites et Polymères (LTC), Ecole Polytechnique Fédérale de Lausanne (EPFL), CH-1015 Lausanne, Switzerland
[b] Tetra Pak (Suisse) SA, Development and Engineering Romont, C.P. 32, CH-1680 Romont, Switzerland

ARTICLE INFO

Article history:
Received 13 February 2009
Accepted in revised form 4 May 2009
Available online 7 May 2009

Keywords:
Silane
UV curing
Gas barrier
Toughness

ABSTRACT

Ultra-thin (10–500 nm) photo-polymerized γ-methacryloxypropyltriethoxysilane (MPMS) and vinyltrimethoxysilane (VTS) layers applied to SiO_2 coatings on polyethylene terephthalate films improved the oxygen barrier performance of the oxide coated films by more than two-fold, and the coating strain to failure from 1.5% to beyond 5%, depending on the processing conditions. The oxygen transmission rate of composite films was measured under tensile strain. The chemical conversion of both MPMS and VTS with two different photoinitiators was studied by means of photo-calorimetry experiments, with attention paid to the influence of temperature, UV-light intensity and photoinitiator concentration. The conversion data were analyzed using an n^{th}-order kinetic model, including an Arrhenius dependence of the temperature and a power-law dependence of the light intensity on the reaction rate. The improvement in mechanical integrity of the silane/silica barrier coating, with a toughness as high as 80 J/m^2 was found to be controlled by the conversion state of the silane.

1. Introduction

Thin, flexible, gas and water vapor barrier coatings based on inorganic as well as hybrid materials on polymer substrates are well established for food packaging applications [1,2]. Single, nano-sized inorganic films (essentially based on metal oxides) produced using vapor deposition techniques present the advantages of being transparent and dielectric i.e., can be used in microwave ovens. The gas permeability of the coated polymer composite film is typically 2–3 orders of magnitude lower than that of the uncoated polymer. The residual gas permeation results from the presence of defects such as deposition instabilities and micro-cracks [3]. These defects, in turn, are crack initiation sites which control the toughness of the barrier coatings and eventually limit their introduction into complex, high rate conversion processes including roll-to-roll methods, folding and welding [4,5]. Considerable effort is ongoing to develop super high barrier coatings to protect emerging flexible electronic devices from environmental degradation. These coatings are based on a variety of oxide and nitride multi-layers, leading to barrier improvement factors over uncoated polymer as high as 10^6 (e.g. [6–10]). In spite of such an outstanding barrier performance, the inorganic coatings remain brittle, with a critical strain for cracking usually in the range from 0.5% to 2% [4]. A major challenge is therefore, to produce a crack resistant, hermetic coating, which can withstand very high strain values (typically 4–5%) without losing its barrier properties. Approaches to this end include coating thickness optimization [4] and internal stress control [11], although these do not significantly improve the barrier performance of the composite film.

In previous studies, hybrid gas barrier materials based on sol–gel [12] and organo-silane [13] process routes have been produced with remarkable combined improvement of barrier and mechanical performance, although these processes were either based on complex multiple step reactions or time consuming thermal polymerization. Silanes are generally used as coupling agents to promote adhesion between polymers and metal surfaces [14–16]. Their utilization dates back to the 1940s when they were processed with fragile glass filaments to reinforce unsaturated polyester resins. The healing of superficial defects in the glass filaments motivated the considerable development of amino-alkoxysilanes [17]. Several works have investigated the reaction of these molecules with hydrated mineral surfaces [18]. Alkoxy silanes can theoretically react with three silanols present on the surface, but in practice, intermolecular silanol condensation also occurs, leading to a layer of siloxane on the mineral surface. The resulting polysiloxane interphase was found to control the permeability and toughness of silica coatings [13]. In this work, the application and thermal cure of amino-alkoxysilanes from dilute solutions in ethanol led to an improvement in barrier properties and critical strain of SiO_2 coatings by factors of 3 and 2 respectively. However, the process of thermal curing was slow (up to 24 h), which is not compatible with high production rate requirements.

The potential of radiation-curable organo-silanes to improve the gas barrier and mechanical properties of inorganic films on polymer substrates is yet to be explored. The key advantage over thermally curable silanes would be the fast conversion processes. The objective of the present study was thus to develop hybrid organic–inorganic

* Corresponding author.
E-mail address: yves.leterrier@epfl.ch (Y. Leterrier).

0257-8972/$ – see front matter © 2009 Elsevier B.V. All rights reserved.
doi:10.1016/j.surfcoat.2009.05.001

coatings based on UV-curable silanes applied to silica films on a polymer substrate, with attention paid to the barrier and mechanical performance of the composite film. To this end, the oxygen barrier properties of the hybrid coatings were investigated using permeation tests carried out under tensile loading, and the chemical conversion state of the silane was analyzed using photo-calorimetry experiments.

2. Experimental

2.1. Materials

The substrate material was a biaxially oriented, 12 μm thick polyethylene terephthalate film (PET, DuPont Mylar®, gauge and type 12.0FA). The oxygen transmission rate (OTR) of the PET film was found to be equal to 120 ± 5 $cm^3/(m^2$ day bar) and its glass transition temperature was equal to 74 °C. The substrate was coated with SiO_2 by plasma-enhanced chemical vapor deposition (PECVD) from hexamethylenedisiloxane as a precursor gas in oxygen plasma [19]. Two coating thicknesses, equal to 10 and 48 nm were produced by varying the amount of monomer in the reactor.

Two types of UV-curable organo-silanes were selected, namely γ-methacryloxypropyl triethoxysilane (MPMS, 99% pure from GE specialty materials, Switzerland) and vinyltrimethoxysilane (VTS, 99% pure from GE specialty materials, Switzerland). Two types of photoinitiators, which matched the photon energy spectra of the UV sources were also selected, namely phenyl bis (2,4,6-trimethyl benzoyl) (PI-1, Irgacure 819, >99% pure from GE specialty materials, Switzerland) and 2-benzyl-2-dimethylamino-1-(4-morpholinophenyl)-butanone-1 (PI-2, Irgacure 369, >99% pure from GE specialty materials, Switzerland), in concentrations ranging from 0.5 wt.% to 4 wt.%. Chemically, PI-1 is a phosphine oxide derivative recommended for clear coat applications and which enables thick sections to be cured, whereas PI-2 contains a tertiary amine, which should catalyze the silane-oxide surface interactions [20,21]. Ethanol (99% pure from ACROS Organics) was used as solvent.

2.2. UV sources

Two different UV sources were used and their spectral characteristics are shown in Fig. 1. A UV-flood lamp was used to cure samples for OTR analysis, with a constant intensity equal to 120 mW/cm^2. A high-pressure mercury lamp with controlled intensity up to 200 mW/cm^2 (Novacure UV 2100, Q series PCA) was used for photo-calorimetry analysis. It was verified that, due to the extremely small thickness of the silane coatings, in the range from 10 to 500 nm, the UV-light intensity, hence the conversion state, was homogenous throughout the coating thickness. To this end, the Beer–Lambert law was used:

$$I(z) = I_o \cdot e^{-2.3\, m_e [\mathrm{PI}] z} \quad (1)$$

Where I_o is the intensity of incident UV light, $I(z)$ is the intensity at depth z, m_e is the molar extinction coefficient equal to 74 L mol^{-1} cm^{-1} [22] and [PI] is the concentration of photoinitiator. For the thicker, 500 nm coating and with a 4 wt.% photoinitiator concentration, the UV intensity differs by less than 1/1000 between the top and the bottom surfaces of the coating.

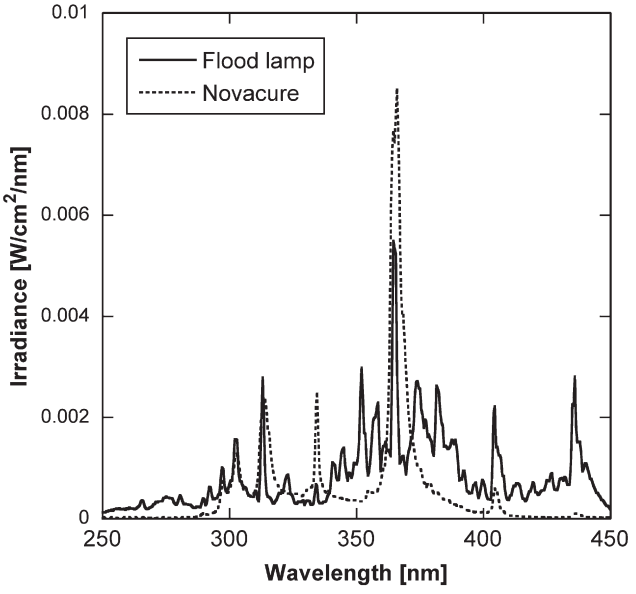

Fig. 1. Spectral characteristics of the UV sources measured with a Solatell Sola-Scope 2000™ instrument (flood lamp used for OTR samples preparation and Novacure for UV-DSC analysis).

2.3. Coating methods

Two coating methods were used, namely spin and roll coating. Spin coating was used to produce samples for standard oxygen transmission rate (OTR) measurements detailed in the next section. Silane solutions in ethanol in concentrations ranging from 1 wt.% to 20 wt.% were spin-coated onto the SiO_2/PET film at 1000 rpm for 20 s, leading to silane coating thickness ranging from approx. 10 nm to 500 nm [23]. Roll coating was used to produce samples for OTR vs. strain tests, also detailed in the following. In roll coating, a liquid film is deposited on a moving substrate by a roller (called a roll applicator) previously impregnated with the liquid solution. This method is more useful than spray or spin coating for the fast treatment of flat surfaces [24]. The advantage of this method lies in its homogeneity and continuity. In fact, the thickness of the coating can be checked precisely and kept constant for a long production time. A roll coating pilot line was built and used for the preparation of roll-to-roll samples as detailed in [25]. This machine was able to accommodate a 120 mm wide film and was operated at a maximum coating speed of 3 cm/s. Tensioners were used to press film against the absorber roller. Counter direction of rotation of roll coater with respect to moving film was chosen to prevent sagging of the film in the UV chamber [26]. The roll coater was impregnated with a 3 wt.% silane solution in ethanol (with 3 wt.% of photoinitiator), which was applied to the moving SiO_2 surface. The machine was equipped with the UV-flood source having a constant intensity equal to 120 mW/cm^2. Temperature during UV curing rose to 60 °C, because of the UV-lamp and no external heating was provided. The thickness of the silane coating obtained at maximum line speed was estimated to be of the order of 100 nm, based on previous data for thermally curable silane coatings also produced from dilute solutions in ethanol [23]. The thickness of these thermally curable silane coatings was measured using transmission electron microscopy and found to be in the range from 10 to 500 nm depending on initial concentration.

In the following, the UV-curable silane/SiO_2/PET composite films with SiO_2 thickness, h_c (10 or 48 nm) obtained at a concentration of x wt.% of silane in ethanol with y wt.% (of x) of photoinitiator (PI-1 or PI-2) will be referred to as x% silane(y% PI-i)/SiO_2-h_c/PET.

2.4. Characterization techniques

2.4.1. Photo-differential scanning calorimetry

Photo-differential scanning calorimetry (photo-DSC) experiments were carried out in TA Instruments DSC-Q 100 apparatus coupled with the Novacure UV 2100 source. Light was transmitted from the instrument to the DSC cell via a 1 m long, 3 mm diameter, dual extended range (250–700 nm) liquid filled light guide. The UV source was also connected to the DSC cell via an event cable that opened and closed the shutter. Exposure times with accuracy of 0.6 s could be

achieved within the temperature range from −50 °C to 80 °C. The calorimeter was calibrated with both zinc and indium. Aluminum pans containing 5–10 mg of sample were used and the analyses were carried out under a continuous flow of U-grade nitrogen, for light intensities in the range from 3 to 40 mW/cm^2, at a constant temperature in the range from 30 °C to 80 °C. In addition, experiments were carried out under air and using an overpressure of 1.5 bar of N_2 to ensure complete absence of oxygen. To quantify the polymerization reactions of MPMS and VTS in terms of double bond conversion, total enthalpy change (ΔH_t) of the reaction was required. For that, thermal polymerization of MPMS and VTS was carried out in thermal DSC using the same Q 100 apparatus at a slow rate of 5 K/min using methylethylketone peroxide (MEKP) as a free radical initiator at a concentration of 4 wt.%. After completion of the reaction, samples from the thermal DSC were taken out and Fourier transform infrared spectroscopy was performed to check the double bond conversion and compare it with enthalpy change (ΔH). Processing of the data led to the following enthalpies for full conversion: $\Delta H_t = -194.65$ J/g for MPMS and $\Delta H_t = -159.58$ J/g for VTS.

2.4.2. X-ray fluorescence spectroscopy

The SiO_2 coating thickness was measured by means of X-ray fluorescence spectroscopy using a Philips Minipal EPX spectrometer, equipped with a 30 kV rhodium anode tube, 5 filters, a helium purge facility, a high resolution solid-state detector and a 12 position movable sample detector. Fused silica and poly(dimethyl siloxane) were used for calibration of Si atom density. Accuracy of the measurement was approximately ±3 nm.

2.4.3. Oxygen transmission rate measurements

The permeation of O_2 was analyzed using a MOCON Oxtran 220 apparatus. This permeation cell calculates the volume of gas that permeates through a unit area of film per unit time and per unit of pressure difference, and stated in cm^3/(m^2 day bar). In this method film samples are mounted in the cell and form a membrane between two chambers. Hermetic sealing is achieved by a combination of a rubber o-ring and vacuum sealing grease. The OTR was measured on 10 cm diameter circular films at 23 °C and 50% relative humidity, with an accuracy of 0.1 cm^3/m^2/day/bar. Prior to the measurement the top and bottom chambers were both flushed with an N_2 flow of 0.5 l/min for 1 h. An O_2 flow of 0.5 l/min was then applied to the top chamber, with the same N_2 flow maintained in the bottom chamber. The OTR was measured using a coulometric sensor under steady state conditions for O_2 flow in the bottom chamber resulting from permeation through the film.

2.4.4. OTR under tensile load

Tensile tests *in-situ* in a gas permeation cell is a novel method that has proved its usefulness to analyze the influence of damage on the permeation through barrier coatings on polymer substrates [27]. The experimental device used in this work consisted of the MOCON cell, equipped with an external traction device. Film samples of size 115×250 mm^2 were made in the pilot line, and were loaded under uniaxial tension by systematically varying the strain stepwise up to 7% (with an accuracy of ±0.5%). At each strain step, the permeation cell was opened and the sample was loaded to obtain a uniform strain state over the whole sample width. Subsequently, vacuum grease was applied on the top and bottom sealing sides, the rubber o-ring was placed and the cell was carefully closed for the next test. As will be detailed in the next section, the OTR of SiO_2/PET films in the tensile test configuration was identical to that of samples tested in the standard configuration of the MOCON cell. These results confirmed the quality of the hermetic sealing and the absence of measurement artifacts, which would have resulted from the mounting of the sample in the external tensile device. The tensile strain was monitored by a micrometer screw attached to the sample grip. Each OTR under strain value was obtained by averaging at least three tests carried out using three different OTR cells equipped with individual straining stages.

3. Results and discussion

3.1. Oxygen permeability analysis of UV-curable silane–silica hybrid coatings

Fig. 2 shows the influence of silane concentration in ethanol on the OTR of silane/SiO_2-48/PET composite films. The tests were carried out after coating and curing MPMS and VTS with 2 wt.% PI-2 on SiO_2-48/PET using a UV intensity of 120 mW/cm^2 for 60 s. The OTR of reference SiO_2-48/PET was found to be equal to 1.8 ± 0.4 cm^3/(m^2 day bar). A two-fold reduction of the gas permeation is evident at concentrations as low as 2 wt.%. Increasing the concentration beyond this value did not improve further the barrier properties. The present results being alike those obtained with thermally curable silanes suggests that similar reactions have occurred as detailed in [23,25]. At 2 wt.% concentration the silane reacted with the hydrated silica surface and formed a cross-linked polysiloxane layer with low oxygen permeability, resulting in the observed two-fold reduction of OTR. As the concentration, hence the thickness of silane was increased, additional condensation reactions took place, leading to a polysilanol network with high oxygen permeability, and the resulting OTR of the composite film was only marginally improved.

The OTR of MPMS and VTS (cured with 3 wt.% PI-1 and PI-2 in the pilot line) coated composite films under tensile strain is compared to the reference SiO_2-48/PET samples in Figs. 3–5. Upon straining, the OTR of the SiO_2-48/PET film progressively increased with a more abrupt rise beyond 2% strain and eventually reached the OTR of the bare PET film. In the present work, the critical strain for the loss of barrier performance was defined as the strain where the OTR reached 3 cm^3/(m^2 day bar), and is equal to approx. 1.5% for the untreated SiO_2-48/PET. Tensile cracks were detected in similar 50 nm thick SiO_2 coatings on PET at 1.8% strain [28] and it is therefore clear that tensile cracks control the loss of barrier properties of the composite film [27]. It is evident from these experiments that the silane treatment was very effective to improve the mechanical integrity of the oxide coating. The critical strain was found to be equal to 2.3% (in the case of PI-1) and to 4.1% (in the case of PI-2) for MPMS. Similar outstanding results were obtained using VTS with the same photoinitiators (Fig. 4).

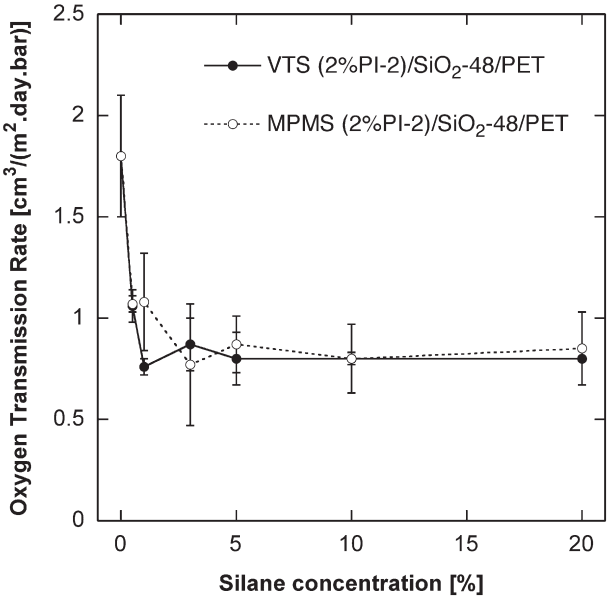

Fig. 2. Influence of initial concentration of VTS and MPMS in ethanol on the oxygen transmission rate of cured silane(2% PI-2)/SiO_2-48/PET films.

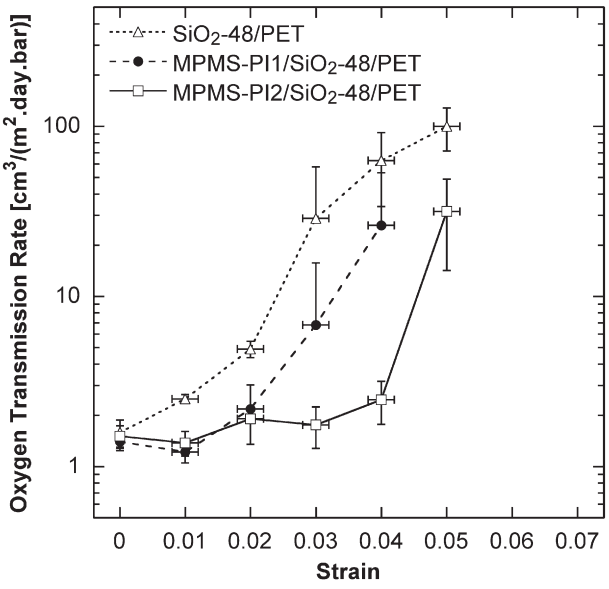

Fig. 3. Influence of strain on the oxygen transmission rate of SiO_2-48/PET and 2% MPMS (2% PI-1,2)/SiO_2-48/PET films.

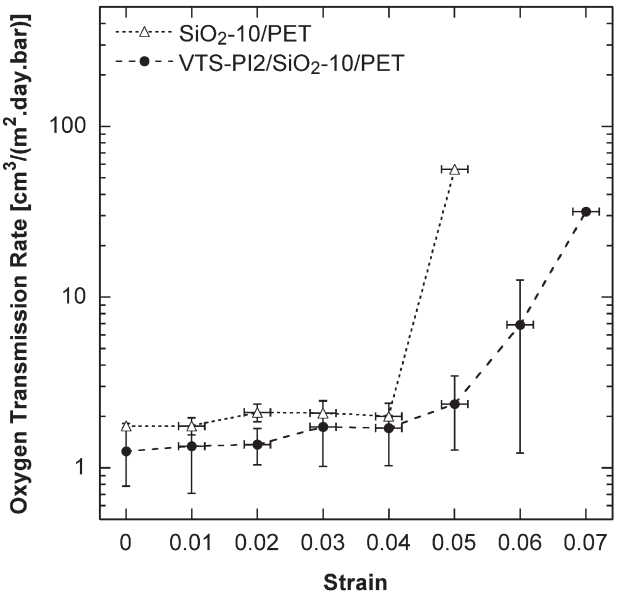

Fig. 5. Influence of strain on the oxygen transmission rate of SiO_2-10/PET and 2% VTS(2% PI-2)/SiO_2-10/PET films.

In this case, the critical strain was equal to 5.1% in the case of PI-2. The critical strain of the 10 nm thick oxide coating was found to be equal to 4.2% i.e., 2.8 times higher than for the 48 nm thick layer. Following fracture mechanics, the intrinsic strain to failure of brittle coatings (i.e., the critical strain corrected for the process-induced internal strain) is expected to scale with the inverse of square root of coating thickness. In the present case, the ratio of critical strain between the 10 nm and the 48 nm thick coatings should be $\sqrt{48/10} = 2.19$. This value is close to the measured ratio of 2.8, the difference presumably resulting from the presence of internal strains. The critical strain of the 10 nm thick coating increased to 5.2% upon treatment with a 3 wt.% VTS solution (Fig. 5). Also interesting is the fact that at all strains levels, the OTR of the silane treated materials was lower than that of the reference SiO_2/PET films.

These exceptional properties obtained for the two types of silanes should be attributed to the formation of a cross-linked polysiloxane network, similarly to the case of thermally curable silanes [13]. In addition, the thermoplastic nature of the UV-curable silanes should be beneficial to improve the toughness of the SiO_x coating. VTS being a lesser sterically hindered molecule than MPMS, should moreover facilitate the polymerization reactions. The better results obtained using PI-2 reflect the catalytic influence of the amine group for the reaction of silanes with the hydrated oxide surface [20,21]. The different behavior obtained with the different silane/PI combinations could eventually result from different degree of conversion of the silanes, as is discussed in the following section.

3.2. Conversion analysis

As shown in Fig. 6, the photoinitiator PI-2 enabled both MPMS and VTS to reach a higher final conversion, compared to PI-1. It was

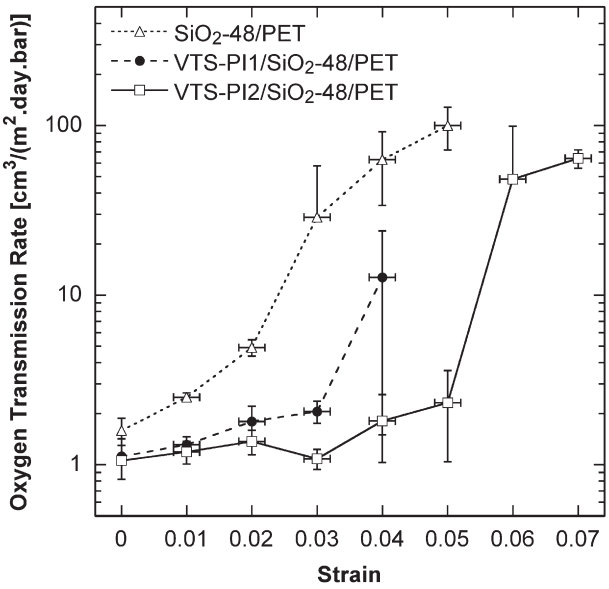

Fig. 4. Influence of strain on the oxygen transmission rate of SiO_2-48/PET and 2% VTS (2% PI-1,2)/SiO_2-48/PET films.

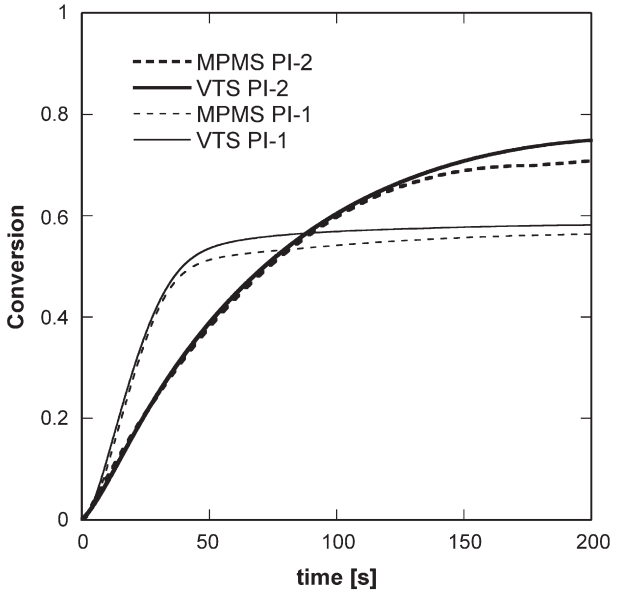

Fig. 6. Photo-conversion of MPMS and VTS with photoinitiators 1 and 2 (concentration equal to 2%), at a UV intensity equal to 20 mW/cm^2 and at 50 °C.

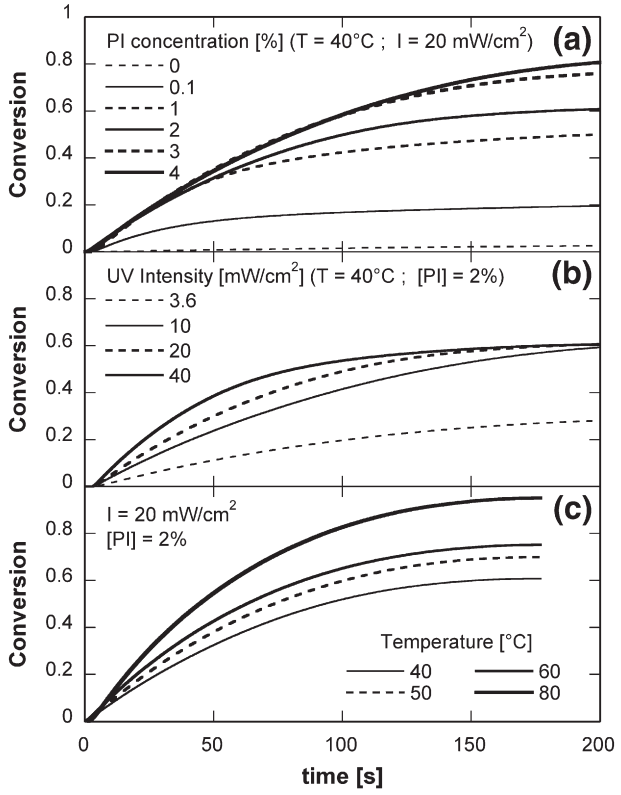

Fig. 7. Influence of photoinitiator concentration (a), UV intensity (b) and temperature (c) on photo-conversion of MPMS.

evident in Figs. 3 and 4 that PI-2 also enabled higher critical strain for the two silanes. In order to clarify the relation between conversion state and critical strain of the silane–silica hybrid coatings obtained using PI-2, the objective of the present analysis is to determine the influence of temperature and UV intensity on the conversion of the silanes. This analysis is required to determine the conversion state of the silane layer produced using the roll coater equipment, i.e., in case of the permeation experiments carried out under tensile strain shown in the previous section.

The conversion state of MPMS and VTS with PI-2 was investigated with systematically changing the photoinitiator concentration, the UV intensity, the temperature and the environment (oxygen and nitrogen). Each factor was varied while keeping the other factors constant, and the results are depicted in Figs. 7 (MPMS) and 8 (VTS). Fig. 7a shows that the final conversion of double bonds in MPMS under 20 mW/cm^2 of UV light increased from 4% to 82% with an increase in initiator from 0 to 4 wt.%. In contrast, the rate of reaction was hardly affected by increasing initiator concentration above 1 wt.%. Fig. 7b highlights the drastic increase of the rate of reaction, and the negligible dependence of the final conversion on UV intensity. Fig. 7c shows that the reaction processes are thermally activated, with a resulting increase of the rate of reaction and of final conversion. The final conversion was also found to be sensitive to the presence of oxygen, with a relative increase of $36\pm14\%$ depending on the temperature from air to a pure nitrogen environment. These confirmed the role of O_2 as an inhibitor for acrylate polymerizations [29].

Results obtained in the case of VTS (Fig. 8) are similar to those obtained for MPMS. The photoinitiator concentration essentially controls the final conversion (Fig. 8a), whereas the UV intensity primarily influences the reaction rate (Fig. 8b). The temperature was found to affect both the rate of reaction and the final conversion, as shown in Fig. 8c.

The conversion rate was calculated from the data shown in Figs. 7 and 8, and was modeled following an n^{th}-order reaction:

$$\frac{d\alpha}{dt} = K\left(1-\frac{\alpha}{\alpha_m}\right)^n \tag{2}$$

where α and α_m represent the conversion and maximum conversion, K and n are the rate constant and reaction order, respectively. Eq. (2) was fitted to the experimental data with adjustable K and n values as shown in Fig. 9. The reaction order values reported in Table 1 are in the range from 0.6 to 1, being almost independent of temperature and increasing with UV intensity. The factor K was expressed to include an Arrhenius dependence of temperature and a power-law dependence of UV intensity:

$$K = K_0 \exp\left\{-\frac{E_a}{RT}\right\} \times I^{\beta} \tag{3}$$

where K_0 is a constant, E_a is the activation energy, R and T are the universal gas constant and absolute temperature, respectively, I is the intensity of the UV source, and β is the power-law exponent and is related to the termination mechanism [29]. For $\beta<0.5$, second order and primary radical termination is predominant. For $0.5<\beta<1$, first order (e.g. trapping of the radical ends in the forming network, or recombination with oxygen) and second order terminations happen in parallel. For $\beta=1$ first order termination is predominant. The values of K obtained from the fits in Fig. 9 are reported in Arrhenius coordinates and are also shown as a function of intensity in Fig. 10. The activation energy E_a and intensity exponent β are reported in Table 2. The activation energy for photo-conversion of MPMS is comparable to that of UV-curing epoxides [30]. The value for VTS which is principally a thermally curable compound is as expected considerably higher. The

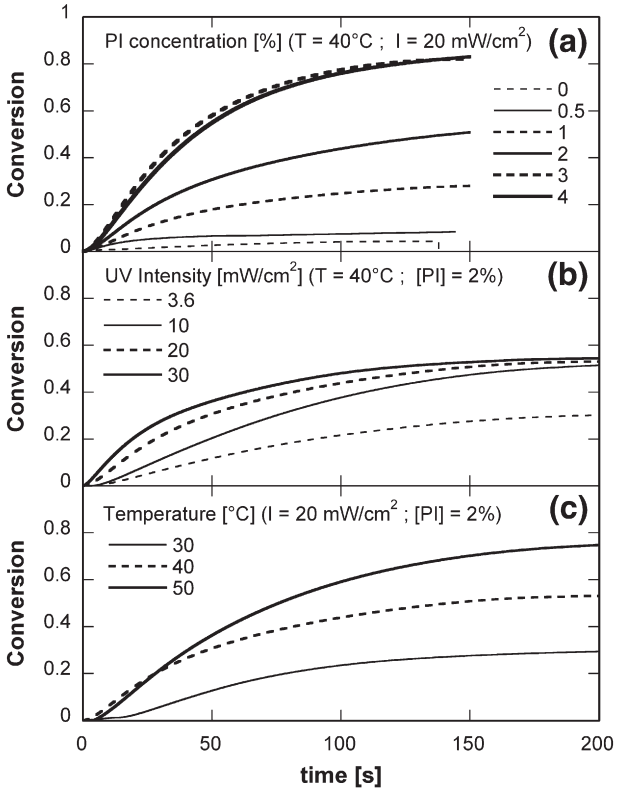

Fig. 8. Influence of photoinitiator concentration (a), UV intensity (b) and temperature (c) on photo-conversion of VTS.

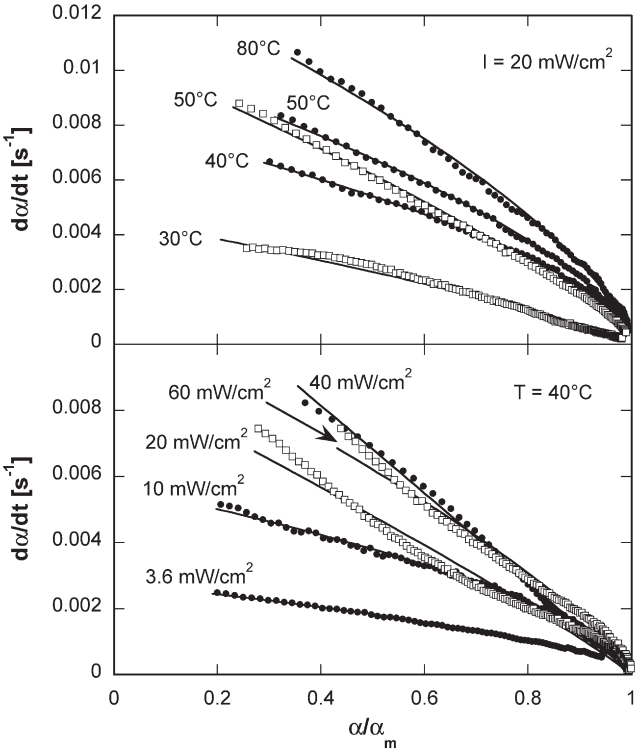

Fig. 9. Comparison between experimental and theoretical (Eq. (2)) conversion rate vs. normalized conversion of MPMS (●) and VTS (□), for a PI-2 concentration equal to 2% and for a range of temperatures (at constant intensity equal to 20 mW/cm^2) and a range of UV intensities (at a constant temperature equal to 40 °C) as indicated in the graphs.

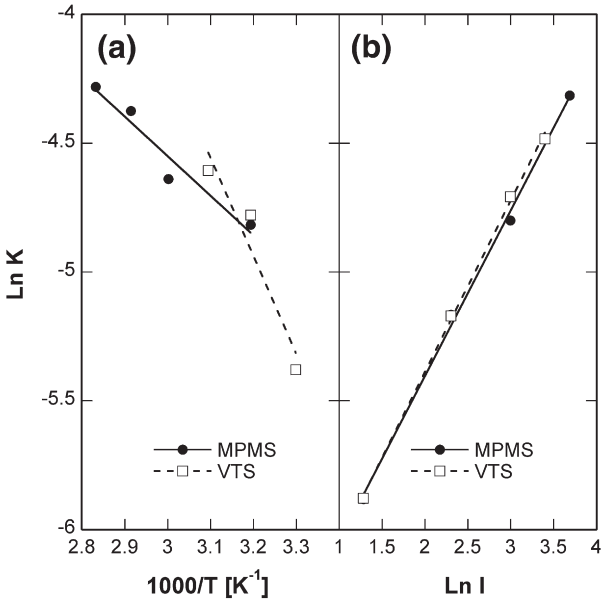

Fig. 10. Arrhenius temperature dependence (a) and power-law intensity dependence (b) of the rate constant K for photo-polymerization of MPMS and VTS.

exponent β was found to be equal within experimental scatter to 0.65 for both MPMS and VTS, i.e. $0.5<\beta<1$. This implies that the photo-conversion of both silanes follows first and second order termination in parallel. The fact that a significant amount of monomolecular termination takes place in addition to bimolecular termination could result from oxygen inhibition processes [29].

To scale up for industrial use, the conversion model can be integrated using the boundary condition $\alpha=0$ at time $t=0$, to evaluate the production rate if the intensity of the lamp, time under UV exposure, temperature and conversion are predetermined. In case of a UV window of 1 m and a UV intensity of 250 W/cm^2, at 50 °C, 90% conversion of VTS can be reached at a production speed of 300 m/min.

3.3. Influence of conversion on toughness of silane–silica gas barrier coatings

In general, the tensile strength and toughness of polymers increase with molecular weight [31,32]. This behavior is evident in the present case of UV-curable silanes, for which the toughness correlates with the conversion level, as shown in Fig. 11. The conversion data in the figure were calculated based on the process conditions (UV intensity equal to 120 mW/cm^2, temperature 60 °C, photoinitiator concentration of 3 wt.%) using the above analysis. The toughness G_c of the SiO_2 and hybrid coatings was derived from an energy release rate analysis for a mode I steady state and through-thickness channeling crack as [33]:

$$G_c = \frac{\pi}{2} h_c E_c \varepsilon_{crit}^2 g(\alpha_D;\beta_D) \quad (4)$$

where h_c is the coating thickness, E_c the coating Young's modulus assumed to be equal to 80 GPa [34], ε_{crit} is the critical strain related to the loss of barrier performance and $g(\alpha_D;\beta_D)$ is a non-dimensional function of the Dundurs parameters α_D and β_D, equal to 5.1 for the SiO_2/PET composite film [33]. The critical strain of the 10 and 48 nm thick oxide coatings was found to be equal to 4.2% and 1.5%, respectively. Using Eq. (4), the corresponding toughness was found to be equal to 11.3 J/m^2 and 6.9 J/m^2.

The toughness of the silane treated silica coatings was also calculated using Eq. (4). In this case, the silane forms a bilayer structure with a polysiloxane monolayer cross-linked on the silica surface, and a polysilanol thermoplastic layer, whose thickness depends on the initial concentration in solution. The polysilanol layer is in a rubbery state with a Young's modulus equal to 30 MPa [35]. This value is many orders of magnitude lower than that of the silica coating, which means that the polysilanol layer will not substantially change the strain energy, hence the cracking strain in the coating. The polysiloxane layer is thin enough and does not significantly change the thickness and modulus of the silica coating. Consequently, the thickness and modulus of the hybrid coating relevant for Eq. (4), hence the function g, were kept equal to those of the untreated oxide coatings. The critical strain of the 10 nm thick hybrid coating was found to be equal to 5.2%, giving a toughness equal to 17.3 J/m^2. The critical strain and toughness of the 3% VTS(3% PI-2)/SiO_2-48 coating were found to be equal to 5.1% and 80.0 J/m^2, respectively.

Table 1
Reaction order of MPMS and VTS for the selected UV intensities and temperatures.

UV silane	UV intensity (mW/cm^2) at 23 °C				Temperature (°C) at 20 mW/cm^2				
	3.6	10	20	40	30 °C	40 °C	50 °C	60 °C	80 °C
MPMS	0.605	0.586	0.719	0.970	–	0.581	0.629	0.620	0.667
VTS	0.592	0.607	0.908	1.006	0.800	0.852	0.776	–	–

Table 2
Activation energy (E_a) and intensity power-law exponent (β) for conversion of UV-curable MPMS and VTS.

UV-silane	Activation energy, E_a [kJ/mol]	Intensity power-law exponent, β
MPMS	12.7 ± 2.2	0.642 ± 0.023
VTS	31.7 ± 9.5	0.664 ± 0.017

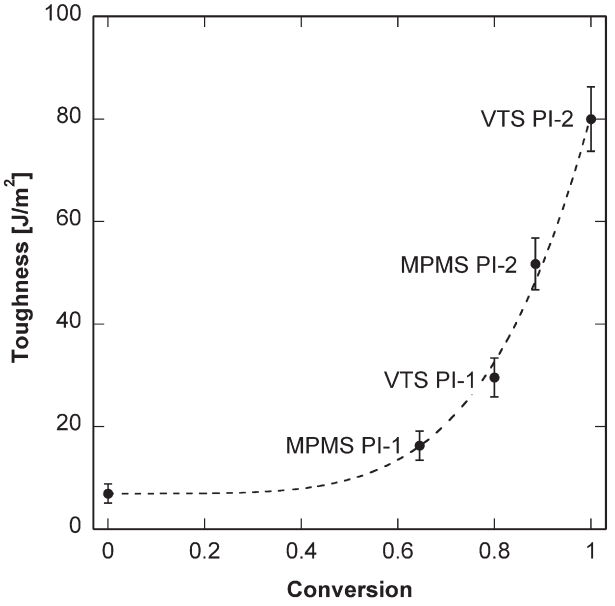

Fig. 11. Influence of conversion state on toughness of silane/SiO_2 coatings. The type of silane (MPMS and VTS) and photoinitiator (PI-1 and PI-2 at a 3 wt.% concentration) is indicated for each data point. The dotted line is a guide for the eye.

The small difference between the critical strains for the 10 nm and 48 nm thick hybrid coatings, or the large difference between the corresponding toughness values are surprising and yet to be elucidated. Accounting for the actual hybrid coating thickness and Young's modulus (using the rule of mixtures with known moduli of silane and oxide) changes the above toughness values by less than 5%. The process-induced internal stress, including shrinkage stress resulting from the polymerization of the silane, cannot explain the small difference in critical strain for the two coating thicknesses. In fact it would favor an increase of critical strain for the thinner coating, which was not the case. The present finding would rather suggest that the microstructure and defect population of the hybrid silane–silica coating, which control the toughness of the material, are very different for the two considered thicknesses, although their oxygen permeation properties are the same within experimental scatter. In spite of this lack of insight into the fundamental failure mechanisms, the present hybrid coatings combine a good barrier performance, an exceptional mechanical integrity and a high conversion rate. The SiO_2 and silane coatings do not embrittle the PET film, which remained ductile and could be strained well beyond yield. In other words the silane treated films are fully compatible with high-rate production of flexible packaging. The healing character of the UV silanes should be useful for roll-to-roll production of durable encapsulation and substrate coatings for flexible electronic devices. These materials would moreover offer a preventive and cost-effective alternative to novel self-healing films described in a recent work [36].

4. Conclusions

The modification of SiO_2 coatings with UV-curable silanes resulted in combined improvement of oxygen barrier (a factor of two) and critical failure strain (a factor of three for VTS) of SiO_2/PET films at a concentration in ethanol as low as 3 wt.%. The key factor, which controls the property improvement of the hybrid UV-curable silane–silica coatings is the chemical conversion state of the silane. A photoinitiator with an amine function led to a higher double bond conversion, presumably due to the catalytic action of the amine. The photo-conversion of MPMS and VTS was analyzed using an n^{th}-order kinetic model (with n in the range between 0.5 and 1, depending on UV intensity and temperature) with a thermally activated rate constant, power-law function of UV-light intensity. The activation energy for VTS was found to be much larger than that of MPMS and the power-law intensity exponent was found to be similar for the two molecules and equal to approx. 0.65. The outstanding critical strain and toughness of the VTS-silica coating, found to be as high as 5% and 80 J/m^2, respectively, make this hybrid coating particularly attractive to avoid premature failure of novel flexible electronic applications.

Acknowledgements

The authors would like to thank the Top Nano 21 initiative of the Swiss Commission for Technology and Innovation (CTI) and the company Tetra Pak, Suisse (SA) for financial support.

References

[1] A.L. Brody, Food Technol. 54 (2000) 72.
[2] J. Lange, Y. Wyser, Packag. Technol. Sci. 16 (2003) 149.
[3] A.P. Roberts, B.M. Henry, A.P. Sutton, C.R.M. Grovenor, G.A.D. Briggs, Y. Tsukahara, T. Miyamoto, J. Membr. Sci. 208 (2002) 75.
[4] Y. Leterrier, Prog. Mater. Sci. 48 (2003) 1.
[5] G. Rochat, Y. Leterrier, J.-A.E. Månson, P. Fayet, Surf. Coat. Technol. 200 (2005) 2236.
[6] M. Schaepkens, T.W. Kim, A.G. Erlat, M. Yan, K.W. Flanagan, C.M. Heller, P.A. McConnelee, Proc. 50th AVS International Symposium, Baltimore, MD, 2003, p. 1716.
[7] J.S. Lewis, M.S. Weaver, IEEE J. Sel. Top. Quantum Electron. 10 (2004) 45.
[8] P. Mandlik, L. Han, S. Wagner, J.A. Silvernail, R.Q. Ma, M. Hack, J.J. Brown, Appl. Phys. Lett. 93 (2008) 203306.
[9] W.S. Jang, I. Rawson, J.C. Grunlan, Thin Solid Films 516 (2008) 4819.
[10] L. Han, P. Mandlik, J. Gartside, S. Wagner, J.A. Silvernail, R.-Q. Ma, M. Hack, J.J. Brown, J. Electrochem. Soc. 156 (2009) H106.
[11] G. Rochat, Y. Leterrier, P. Fayet, J.-A.E. Månson, Thin Solid Films 484 (2005) 94.
[12] K.H. Haas, S.A. Schwab, K. Rose, Surf. Coat. Technol. 111 (1999) 72.
[13] J. Bouchet, G. Rochat, Y. Leterrier, J.-A.E. Månson, P. Fayet, Surf. Coat. Technol. 200 (2006) 4305.
[14] E. Nishio, N. Ikuta, H. Okabayashi, J. Anal. Appl. Pyrolysis 18 (1991) 261.
[15] P. Zinck, H.D. Wagner, L. Salmon, J.F. Gérard, Polymer 42 (2001) 6641.
[16] A.C. Miller, J.C. Berg, Compos., Part A Appl. Sci. Manuf. 34 (2003) 327.
[17] P. Zinck, M.F. Pay, R. Rezakhanlou, J.F. Gérard, J. Mater. Sci. 34 (1999) 2121.
[18] E.P. Plueddmann, Silane Coupling Agents, Plenum Press, New York, 1990.
[19] M. Creatore, F. Palumbo, R. d'Agostino, P. Fayet, Surf. Coat. Technol. 142 (2001) 163.
[20] R.L. Kaas, J.L. Kardos, Polym. Eng. Sci. 11 (1971) 11.
[21] C. Chiang, H. Ishida, J.L. Koenig, J. Colloid Interface Sci. 74 (1980) 396.
[22] T. Scherzer, U. Decker, Nucl. Instrum. Methods Phys. Res., B 151 (1999) 306.
[23] B. Singh, J. Bouchet, G. Rochat, Y. Leterrier, J.-A.E. Månson, P. Fayet, Surf. Coat. Technol. 201 (2007) 7107.
[24] S. Paul, Surface Coatings, Science and Technology, John Wiley & Sons, New-York, 1985.
[25] B. Singh, J. Bouchet, Y. Leterrier, J.-A.E. Månson, G. Rochat, P. Fayet, Surf. Coat. Technol. 202 (2007) 208.
[26] J. Greener, S. Middleman, Ind. Eng. Chem. Fundam. 20 (1981) 63.
[27] M. Yanaka, B.M. Henry, A.P. Roberts, C.R.M. Grovernor, G.A.D. Briggs, A.P. Sutton, T. Miyamoto, Y. Tsukahara, N. Takeda, R.J. Chater, Thin Solid Films 397 (2001) 176.
[28] Y. Leterrier, J. Andersons, Y. Pitton, J.-A.E. Månson, J. Polym. Sci., B, Polym. Phys. 35 (1997) 1463.
[29] E. Andrzejewska, Prog. Polym. Sci. 26 (2000) 605.
[30] J.D. Cho, J.W. Hong, Eur. Polym. J. 41 (2005) 367.
[31] H.H. Kausch, Polymer Fracture, Springer-Verlag, Berlin, 1978.
[32] I. Narisawa, A.F. Yee, Crazing and fracture of polymers, in: R.W. H.P., Cahn, E.J. Kramer (Eds.), Materials Science and Technology, a Comprehensive Treatment, Structure and Properties of Polymers, vol. 12, VCH, New-York, 1993.
[33] J.L. Beuth, Int. J. Solids Struct. 29 (1992) 1657.
[34] Y. Leterrier, Y. Wyser, J.-A.E. Månson, J. Hilborn, J. Adhes. 44 (1994) 213.
[35] J. Bouchet, G.M. Pax, Y. Leterrier, V. Michaud, J.-A.E. Månson, Compos. Interfaces 13 (2006) 573.
[36] H.A. Liu, B.E. Gnade, K.J. Balkus, Adv. Funct. Mater. 18 (2008) 3620.